Published in final edited form as:
Neuron. 2014 August 6; 83(3): 708–721. doi:10.1016/j.neuron.2014.06.021.

Selective responses to tonic descending commands by temporal summation in a spinal motor pool

Wei-Chun Wang[1] and **David L. McLean**[1,2,*]

[1]Interdepartmental Neuroscience Program, Northwestern University, Evanston, IL 60208, USA

[2]Department of Neurobiology, Northwestern University, Evanston, IL 60208, USA

Summary

Motor responses of varying intensities rely on descending commands to heterogeneous pools of motoneurons. In vertebrates, numerous sources of descending excitatory input provide systematically more drive to progressively less excitable spinal motoneurons. While this presumably facilitates simultaneous activation of motor pools, it is unclear how selective patterns of recruitment could emerge from inputs weighted this way. Here, using *in vivo* electrophysiological and imaging approaches in larval zebrafish, we find that, despite weighted excitation, more excitable motoneurons are preferentially activated by a midbrain reticulospinal nucleus, by virtue of longer membrane time constants that facilitate temporal summation of tonic drive. We confirm the utility of this phenomenon by assessing the activity of the midbrain and motoneuron populations during a light-driven behavior. Our findings demonstrate that weighted descending commands can generate selective motor responses by exploiting systematic differences in the biophysical properties of target motoneurons and their relative sensitivity to tonic input.

Introduction

All movements must be executed with varying degrees of precision and strength. Our best understanding of how graded movements are produced arises from studies of mammalian hindlimb motoneurons, where increases in movement intensity are accomplished by the addition of larger, less excitable motor units capable of generating more powerful muscle contractions (Burke, 1979; Cope and Pinter, 1995; Enoka and Stuart, 1984; Heckman and Enoka, 2012; Mendell, 2005). The appropriate recruitment of these motor units relies on descending inputs, whose activity generates motor responses matched to behavioral demands (Alstermark and Isa, 2012; Drew et al., 2004; Dubuc et al., 2008; Le Ray et al., 2011; Lemon, 2008). Studies of a variety of descending inputs have revealed that less excitable hindlimb motoneurons receive greater effective excitatory synaptic input than

*Correspondence: david-mclean@northwestern.edu.

more excitable ones (Binder et al., 1998; Burke et al., 1976; Grillner et al., 1970, 1971; Powers et al., 1993; Westcott et al., 1995). One unresolved issue that has been technically difficult to address *in vivo* is how weighted descending inputs optimized for synchronous activation of motor pools could generate differential activation of spinal motoneurons, as required for gradations in movement intensity. Here, we address this issue by examining the descending control of axial motor pools in larval zebrafish.

As in all vertebrates, in zebrafish larvae descending commands exert differential control of movement intensity, from powerful escape responses to precise capture maneuvers (Borla et al., 2002; Eaton et al., 1984; Gahtan et al., 2005; Liu and Fetcho, 1999). To do so, they utilize identified spinal motoneurons organized from ventral to dorsal according to their size, excitability, target musculature, and sequence of recruitment (McLean et al., 2007; Menelaou and McLean, 2012). Specifically, the ventral-most cells in the pool are the most excitable and are recruited first. This topographic pattern of recruitment provides a unique opportunity to examine how descending inputs interact with a heterogeneously excitable motor pool to generate appropriately graded actions. To this end, we focused on descending inputs arising from the nucleus of the medial longitudinal fasciculus (nMLF), a spatially compact, readily identifiable source of reticulospinal drive implicated in visuomotor behaviors (Gahtan and O'Malley, 2003; Gahtan et al., 2005; Kimmel et al., 1982; Orger et al., 2008).

We demonstrate that the preferential recruitment of more excitable motoneurons can be achieved by weighted drive from an identified nMLF neuron to the axial motor pool, because commensurate differences in membrane time constants facilitate the temporal summation of tonic inputs. We then explore the activity patterns within the nMLF and spinal motoneurons in response to changes in ambient light levels to assess the behavioral relevance of this phenomenon. Increases and decreases in whole-field illumination are sufficient to make identified neurons within the nMLF fire tonically at frequencies that lead to temporal summation, and also to generate preferential activation of more excitable, ventral motoneurons. Thus, our findings now provide a generalizable mechanism for graded recruitment patterns via weighted descending inputs that relies on the biophysical properties of target motoneurons and their sensitivity to tonic drive.

Results

Anatomical and Physiological Evidence for nMLF to Motoneuron Connections

We first examined the axon collateral distribution in the spinal cord of nMLF neurons, including the identified MeM (Medial-Medial), MeLc (Medial-Lateral, caudal), and MeLr (Medial-Lateral, rostral) neurons (Figure 1A1–3). Neurons within the nMLF were first retrogradely labeled by dye injection into the spinal cord and then one of the three identified nMLF somata was filled with a different colored dye by single cell electroporation (Figure 1B–C). Given the known dorso-ventral patterning of spinal motoneuron recruitment (McLean et al., 2007; Menelaou and McLean, 2012), we examined axon collateral distributions parasagitally (Figure 1D1–4), and their dorso-ventral distribution was analyzed between body segments 5–14, where the height (distance between the dorsal and ventral boundaries) of the spinal cord is relatively constant. In 5 fish, 2 of the nMLF neurons

(MeLr/MeLc, MeLr/MeM, or MeLc/MeM) were electroporated using different colored dyes for direct comparison of projection patterns within fish (Figure 1B–C, E–F).

While all identified nMLF neurons had main axons that descended ventro-medially in the spinal cord, there were differences in the dorso-ventral distribution of collaterals arising from the main axon. Compared to the MeLr, the MeM and MeLc axon collaterals extended more dorsally in the spinal cord (Figure 1E–H). Like the MeLr, smaller, non-identified neurons within the nMLF had axon collaterals that remained ventral (Figure S1). Due to the finer processes of the smaller cells, we could not be totally confident that their axons were completely filled. However, for the spinal projection patterns of the larger MeM, MeLc, and MeLr neurons, where we could be confident of complete filling, the differences in dorso-ventral projection held true for pooled data from multiple fish (Figure 1I, n = 5 for each cell type). Thus, the most dorsal axon collaterals (above spinal dorso-ventral division 0.5) were exclusively from the MeM and MeLc neurons.

To relate these projection patterns to potential connections with axial motoneurons, we performed single cell electroporations of the MeM, MeLc, and MeLr neurons in the *parg*^{mn2Et} enhancer trap line, in which motoneurons are labeled with GFP (Figure 2A1–2). The MeM and MeLc both had extensive axon collaterals that reached the dorsal-most aspect of the axial motor column (Figure 2B1 and C1). There were also extensive ventral collaterals (Figure 2B1 and C1), where motoneurons are more numerous (Menelaou et al., 2014). Collaterals throughout the dorso-ventral axis penetrated the soma layer, which is most obvious from a coronal view (Figure 2B2 and C2). Digital reconstructions followed by registration to anatomical landmarks confirmed this pattern and also demonstrated that both the MeM and MeLc had bilateral projections (Figure 2E). Thus one of the potential targets included large, dorsally located, early born ‘primary’ motoneurons (PMns; Myers, 1985). To confirm this potential connection, we performed *in vivo* paired patch clamp recordings from the large identified nMLF neurons and large identified PMns (Figure 2F). Consistent with the anatomical observations, we found evidence for direct synaptic connections to PMns from the MeM and MeLc neurons (Figure 2G–H). Current-evoked firing in the MeM or MeLc neurons elicited excitatory post-synaptic potentials (EPSPs) in PMns with two components (Figure 2G–H). The early component had a short, relatively fixed latency in both the MeM (mean ± SEM, 0.92 ± 0.10 ms, coefficient of variation or CV = 0.04) and MeLc (1.05 ± 0.07 ms, CV = 0.04), and a relatively fixed amplitude in both classes (MeM, 1.89 ± 0.29 mV, CV = 0.08; MeLc, 2.39 ± 0.61 mV, CV = 0.07; n = 4 MeM-PMn and 9 MeLc-PMn pairs). In addition, the early component followed MeM and MeLc action potentials reliably without failure, even at extremely high firing rates (up to 500 Hz). These features suggest a monosynaptic, electrical connection between the MeM and MeLc neurons and PMns. The later component occurred less reliably and had larger variability in both latency (MeM, 1.62 ± 0.07 ms, CV = 0.13; MeLc, 1.88 ± 0.36 ms, CV = 0.24) and peak amplitude (MeM, 1.23 ± 0.11 mV, CV = 0.20; MeLc, 1.84 ± 0.17 mV, CV = 0.16), which is more consistent with a chemical connection (Kimura et al., 2006; McLean et al., 2008).

In contrast to the MeM and MeLc, the more ventrally located MeLr axon collaterals ramified laterally in the neuropil layer (Figure 2D1–2, E), as did the collaterals of the smaller nMLF cells (Figure S1). However, since the dendrites and axons of all axial

motoneurons intermingle in the neuropil (Kishore and Fetcho, 2013), this did not rule out the possibility that the MeLr and smaller nMLF cells could still make contact with more dorsal motoneurons. Consistent with this idea, we found connections between MeLr neurons and PMns (Figure 2I), which also contained an early component with a relatively fixed latency (1.28 ± 0.22 ms, CV = 0.05) and amplitude (1.07 ± 0.14 mV, CV = 0.08) and a later component with more variable latency (2.05 ± 0.32 ms, CV = 0.13) and amplitude (0.92 ± 0.06 mV, CV = 0.32; n = 3 MeLr-PMn pairs). Despite the greater likelihood that MeLr-PMn connections were axonal and/or dendritic and thus more distant from the somatic recording site, we found no significant differences in the amplitude of the early component EPSP among the three identified neurons (Figure 2J). Only the late component demonstrated any statistically significant difference, and this was restricted to the MeLc-PMn connection, when compared to the MeM and MeLr pairs (Figure 2J). Thus, the anatomical and physiological data suggest that nMLF neurons have the capacity to make connections to neurons distributed throughout the axial motor pool, which include the smaller, more ventrally distributed, later born ‘secondary’ motoneurons (SMns; Myers, 1985). We next investigated the nature of connectivity between PMns and SMns and focused on connections arising from the MeLc neuron, due to its more superficial, accessible location in the nMLF, and the greater likelihood of finding somatic connections throughout the axial motor pool based on its anatomy.

Paired Recordings Reveal the Nature of nMLF and Spinal Motor Pool Connectivity

To reveal the nature of connectivity between the MeLc neuron and the axial motor pool, we targeted PMns and SMns located between body segments 10–13. Similar to the MeLc-PMn connection, the MeLc-elicited EPSPs in SMns also contained an early, reliable component with relatively constant latency (1.20 ± 0.05 ms, CV = 0.06) and amplitude (2.57 ± 0.38 mV, CV = 0.07; n = 13 MeLc-SMn pairs). There was also a later, less reliable component with more variable latency (2.25 ± 0.09 ms, CV = 0.26) and amplitude (2.76 ± 0.41 mV, CV = 0.25; n = 10 MeLc-SMn pairs). In both PMns and SMns, dual component EPSPs were resistant to a reduction in the likelihood of neurotransmitter release after perfusion of high-divalent cation extracellular solution (Figure 3A–B), consistent with a monosynaptic connection (Frankenhaeuser and Hodgkin, 1957). Furthermore, the later component in both classes was sensitive to a mixture of the glutamate receptor antagonists NBQX/AP5, consistent with a glutamatergic, chemical synaptic connection (Figure 3A–B). Critically, however, in control solutions the amplitude of both the electrical and glutamatergic components was indistinguishable between PMns and SMns, despite dramatic differences in input resistance (Rin) between the two populations (Figure 3E1, G1). This is consistent with experiments that failed to demonstrate any difference in EPSP amplitudes related to Rin in limb motoneurons (Burke et al., 1976; Grillner et al., 1970, 1971). In addition, although the chemical component was highly variable, we found that it was more reliable in PMns than in SMns (Figure 3F). Both observations are consistent with the idea that descending drive is weighted such that less excitable motoneurons receive more excitation, and we now extend this observation to individual reticulospinal inputs.

Despite similarities in the amplitudes of MeLc-evoked EPSPs in PMns and SMns, we did observe differences in their waveforms (Figure 3C–D). Both the electrical and chemical

components of EPSPs in SMns were broader and had a slower decay than EPSPs in PMns. To quantify this observation, we took advantage of the variable reliability of the later chemical component to separately analyze PSPs with purely electrical components and those with clear chemical components. Specifically, we focused on how the following features of EPSPs related to the Rin of spinal motoneurons: 1) 10–90% rise time, 2) half width, 3) decay time constant (Figure 3E2–4). For purely electrical components, the rise time, half width, and decay time constant increased with motoneuron Rin (Figure 3E2–4). We confirmed that this observation was not contaminated by a residual chemical contribution by measuring the same properties in the presence of NBQX/AP5 (Figure S2). Although the early electrical component precluded measurement of the rise time of the chemical component, this same pattern was evident when we analyzed PSPs containing a clear chemical component (Figure 3G2–3). The systematic broadening of the chemical as well as the electrical component is most simply explained by longer membrane time constants, although it is possible that SMns also express a higher ratio of NMDA to AMPA receptors or generally have slower post-synaptic kinetics. Furthermore, in the MeM- and MeLr-PMn pairs, MeM- and MeLr-elicited EPSPs also show narrower waveform and a fast decay similar to the MeLc-elicited EPSPs in PMns, suggesting that this feature is not restricted to the MeLc-motoneuron connection and instead reflects an intrinsic attribute of PMns (Figure S2).

The slower decay of EPSPs in higher Rin SMns could provide a larger time window for EPSP summation. To test whether differences in temporal summation could indeed generate differences in motoneuron recruitment, we evoked action potentials up to 600 Hz in the MeLc neuron (‘Pre’) using current steps and examined whether the motoneuron (‘Post’) could be driven to fire (Figure 4A–B). In the 9 MeLc-PMn pairs, we never observed firing in the PMn (Figure 4A). On the other hand, for 3 MeLc-SMn pairs, firing the MeLc neuron could make the SMn fire (Figure 4B). When we examined the response of the PMn and SMn at the onset of the current step (Figure 4C, D), we found that at low MeLc firing rates PMns and SMns showed a relatively equivalent amount of summation, as quantified by generating a slope from the peak of the first two PSPs in the train (Figure 4E). However, while the PMn exhibited little increase in slope at progressively increasing MeLc firing rates (low gain), in the SMn the increased temporal summation produced an ever-increasing slope with increasing MeLc firing rates (high gain). We then compared the relative gain of responses to current steps in 8 motoneurons where the MeLc was driven to fire over a comparable frequency range (100–600 Hz). The excitatory gain systematically increases with increases in the EPSP decay time constant (Figure 4F), as expected if Rin was contributing to the efficacy of temporal summation.

The contribution of Rin to temporal summation of EPSPs assumes that there are systematic differences in membrane time constant related to Rin. To examine the relationship between membrane time constant and motoneuron Rin, we performed whole-cell recordings from individual spinal motoneurons (n = 41), which covered the full range of motoneuron Rin (~30–1000 MΩ; Menelaou and McLean, 2012). A brief (1 ms) hyperpolarizing current was delivered and membrane potential decay was fitted with a single exponential equation to calculate the time constant. Similar to the EPSP decay time constant, the membrane decay time constant measured somatically also increased with motoneuron Rin (Figure 4G). Thus,

the entire motor pool exhibits a gradient in both Rin and membrane time constant that would provide systematically greater temporal summation of excitatory inputs.

The findings thus far suggest that nMLF neurons have the potential to make contacts with spinal motoneurons throughout the dorso-ventral axis either via somatic or axonal/dendritic connections. In addition, our assessment of MeLc output to axial motoneurons suggests that it is biased to less excitable cells, but can result in selective activation of more excitable ones via temporal summation. To do so, however, the MeLc must fire tonically at frequencies exceeding 200 Hz (Figure 4B, D). Given that these are extremely rapid rates of firing, it is not clear if this would occur naturally. To begin to address this question, we investigated in more detail the activity patterns of neurons within the nMLF during motor behavior.

Calcium Imaging During Sudden Changes in Illumination

Our first goal was to identify a sensory stimulus that would drive reliable activation of the nMLF. Given its acknowledged sensitivity to visual stimuli (Orger et al., 2008; Sankrithi and O'Malley, 2010), we chose a simple, controllable source of photic stimulation, namely a light emitting diode (LED), to generate sudden increases and decreases in whole-field illumination. We then utilized calcium imaging to assess activity in the nMLF combined with peripheral motor nerve recordings to monitor motor responses (Figure 5A). In these experiments, the fish is immobilized with α-bungarotoxin and the bursts of motor activity that would normally drive movements ('fictive') can be monitored (Figure 5A). In response to an LED, motor activity was reliably observed in response to both light onset and offset (Figure 5B). In some instances, spontaneous motor activity unrelated to light stimuli was also observed (gray arrowheads, Figure 5B). There was no significant difference in the delay related to whether the light was turned on or turned off (light onset, 219.32 ± 17.91 ms; light offset, 215.11± 11.60 ms; Mann-Whitney U test, $p > 0.05$, $n = 10$ fish).

Next, to examine the recruitment pattern of neurons within the nMLF, the location of cells was normalized using the midline of the brain and the center of the MeLr neuron as medio-lateral (M-L) references (Figure 5C). While the responses to light onset within the nMLF were highly variable (Figure 5E), the vast majority exceeded the 9% ΔF/F value, which can be used as a conservative estimate of suprathreshold activity (Figure S3; Bhatt et al., 2007; Fetcho and O'Malley, 1995). Averages of responses binned according to M-L location revealed significantly less activity in neurons found in the most medial bin and those found in the 4 most lateral bins (Figure 5G). The MeM, which is located in the most medial bin, also responded less robustly than either the MeLr or MeLc in response to light onset (Figure 5G). In contrast, responses to light offset were more homogeneous (Figure 5E), with no significant difference related to binned M-L location or neuron identity (Figure 5G).

These data suggest that whole field changes in illumination are a reliable means to generate motor responses and to activate neurons distributed throughout the nMLF. How might this compare to responses in the axial motor pool? When we examined the recruitment patterns of axial motoneurons distributed throughout the dorso-ventral plane (Figure 5D), both light onset and offset consistently activated predominantly ventral motoneurons (Figure 5F, H). The contrasting responses of the nMLF and axial motor pools are readily apparent by representing activity as a simple reliability index, quantified as the percentage of responses

≥ 9% ΔF/F to light stimuli, and represented as a 3D-registration with response reliability color-coded (Figure 5I, J). In addition, the 3-D registration demonstrates the clear bilaterality of the response to light and confirms there are no hidden patterns along the dorso-ventral axis on the nMLF, or the medio-lateral axis in the spinal cord. Taken together, these data suggest that nMLF neurons respond to light stimuli more reliably and homogeneously than do spinal motoneurons, where only the most ventral, excitable cells are activated.

Electrophysiological Recordings from Identified nMLF Neurons

Having identified a sensory stimulus that would reliably engage the nMLF, but preferentially engage more excitable motoneurons, we next examined the firing patterns of nMLF neurons related to motor output, by performing *in vivo* cell-attached and whole-cell patch-clamp recordings from the three identified nMLF neurons in conjunction with peripheral motor nerve recordings. In response to light onset and offset, the MeM, MeLc, and MeLr neurons all fired action potentials (Figure 6A–C). In most cases (n = 175/186 trials from 17 cells), the nMLF neurons started to fire before swimming was initiated, as demonstrated in the raster plots and histograms relating spiking to fictive motor bursts (Figure 6B, C). In instances when nMLF neurons did not fire in response to light, there was an increase in synaptic drive shortly after light onset and offset (Figure S4). Subthreshold activity was more frequently observed in the MeM and MeLc (MeM, n = 51/133 trials from 8 cells; MeLc, n = 42/138 trials from 9 cells; MeLr, n = 6/84 trials from 9 cells), which displayed low rates of spontaneous firing compared to the MeLr. Unlike spinal motor pools (McLean et al., 2007), we found no significant difference in their Rin that could explain this observation (MeM, 96 ± 16 MΩ, n = 10; MeLc, 73 ± 5 MΩ, n = 18; MeLr, 100 ± 10 MΩ, n = 8; Mann-Whitney U-tests with Bonferroni corrections, $p > 0.05$). Critically, however, despite differences in firing patterns, all three identified nMLF neurons could fire at rates exceeding 400 Hz, which is higher than the minimum frequency at which temporal summation can activate highly excitable SMns (Figure 6D).

The early onset of firing coupled with the high firing rates suggested that the nMLF neurons likely play a role in short-latency activation of motoneurons in response to photic cues. While our data cannot distinguish between retinal or pineal sensory input to the nMLF, the clear synaptic responses following LED stimuli rule out intrinsic photosensitivity (Fernandes et al., 2012).

Next, to assess directly whether natural light stimuli and stimulation of the nMLF elicited similar responses in motoneurons, we examined firing evoked by the LED in paired recordings from the MeLc and spinal motoneurons. Among our paired recordings where stimulation of the MeLc could make the SMn fire (supra-threshold pair; n = 3), we also observed firing in SMns in response to light that was preceded by PSPs arising from the MeLc (Figure 7A). Interestingly, in these recordings high-frequency tonic firing in the MeLc was also associated with high-frequency tonic firing in the SMn. The tonic response to light stimuli appeared to be linked to whether stimulation of the MeLc alone was sufficient to get the SMn to fire. In SMns that also responded to light, but could not be driven by the MeLc (sub-threshold pair; n = 2), the response was more rhythmic (Figure

7A). In PMns, none could be activated by firing the MeLc alone (n = 6), and only 1 fired in response to light.

The apparent dependence of light-evoked spiking in SMns on the strength of MeLc input led us to investigate in more detail the nature of motor responses to light. To do so, we performed whole-cell patch clamp recordings while simultaneously monitoring motor nerve activity. We focused on motoneurons that exhibited clear PSPs preceding the initiation of motor activity in response to light (n = 25 cells). As mentioned above, spontaneous motor activity was often observed in the absence of light stimuli (Figure 5B). The activity was consistent with 'fictive' swimming behavior, characterized by cyclical bursts of motor activity that would drive rhythmic tail contractions (Figure 7B–D, left). When we examined the activity of motoneurons and motor nerves during light stimuli, we found that activity in response to light was more robust, as reflected by more spiking in the motoneurons and motor bursts of larger amplitude and longer duration (Figure 7B–D, right). As with the paired recordings, we found examples of SMns that fired tonically (n = 8) and ones that fired more rhythmically (n = 12; Figure 7E–F). Tonic firing is evident as the occurrence of spikes outside the duration of peripheral motor bursts (Figure 7E, gray arrowheads). In contrast, PMns were rarely activated by light (n = 1 of 5; Figure 7G), suggesting that the modulation of the motor pattern was largely due to modulation of SMn activity.

Critically, the SMns that were driven tonically had higher Rins than those with more rhythmic behavior (tonic, 421 ± 47 MΩ; rhythmic, 291 ± 29 MΩ; Mann-Whitney U-test, $p < 0.05$). This suggests that tonic SMns, due to their greater excitability, are more sensitive to inputs from the nMLF, which are also presumably tonic in nature. To quantify the rhythmicity of firing, we normalized the occurrence of spikes to the cyclical swimming rhythm recorded from the peripheral motor nerve on a polar plot (0 = start of the cycle, 1 = end). Indeed, spikes from tonically firing SMns were more broadly distributed throughout the swim cycle than spikes from rhythmically firing SMns (Figure 7H). A similar examination of the spiking behavior in the MeM, MeLc, and MeLr demonstrates that spikes occur with equal probability throughout the swim cycle (Figure 7H), confirming their tonic nature.

While the single nerve recordings were consistent with swimming, we could not rule out the possibility that the increased bursting of motor nerves represented a transition to struggling behavior (Liao and Fetcho, 2008), during which the nMLF is known to be active (Sankrithi and O'Malley, 2010). During struggling, increased motor bursts are also characterized by left-right alternation, however the activity passes from tail to head. Therefore, we performed multi-site peripheral nerve recordings and examined both spontaneous motor activity and responses to light (Figure 8A). Spontaneous motor activity demonstrated all the hallmarks of swimming, namely alternation across the left and right sides and a head to tail delay (Figure 8B). During light evoked activity, we observed principally two patterns. The most common pattern was a bilateral, symmetrical increase in motor burst durations (n = 1,518 of 1,601 cycles from 8 fish), which began to occupy up to 50% of the swim cycle (i.e., duty cycle), but remained alternating and passed from head to tail (Figure 8C, left). In some occasions (n = 83 of 1,601 cycles from 8 fish), we also observed unilateral, asymmetric increases in burst durations that well exceeded a 50% duty cycle, but exhibited a rostro-caudal delay (Figure

8C, right). In these cases, there was a complete lack of activity on the other side and the time between successive motor bursts (cycle period) exceeded 50 ms (Figure 8D), which more closely resembles turning behavior (Huang et al., 2013). As a consequence of increased motor bursts, a comparison of duty cycle in spontaneous versus light-driven activity revealed a significant shift to the right (Figure 8E). These data suggest that in addition to initiating activity within the motor pool, tonic activity within the nMLF likely acts to modulate the activity of SMns during ongoing swimming in response to photic cues.

Discussion

The primary motivation for this study was the observation that many major descending pathways important for motor control have weighted outputs to limb motor pools, where motoneurons with lower Rin receive a greater amount of excitatory drive. The utility of this pattern with respect to the synchronization of motor pools during the initiation of fast, powerful movements is well acknowledged (Burke, 1979; Hultborn et al., 2004). What was less clear, however, was how this pattern could produce graded motor output, since drive is effectively normalized to cellular excitability and thus equalizes its influence across motor pools. This is important, because numerous studies have implicated descending inputs in the execution of movements over a wide range of speeds and intensities. Our work now provides a relatively simple solution that helps reconcile these observations. Weighted inputs optimized for synchronous activation of motor pools can also generate preferential activation of subsets of more excitable neurons based on their more effective temporal summation of tonic drive.

To reveal this pattern, we took advantage of our ability to perform recordings from motoneurons of varying excitability that innervate the same axial muscle and then record from a single, common source of descending input that is easily identifiable from fish to fish. In contrast, demonstrations of normalized distribution of effective synaptic currents in mammals used bulk electrical stimulation, which will also activate indirect pathways that impinge upon motoneurons (Binder et al., 2002). This suggests that multiple converging inputs are similarly scaled to excitability. Consequently, it is likely that regardless of the source of excitatory input, higher Rin motoneurons with longer membrane time constants will be the first to be engaged by tonic sources of drive. Consistent with this idea, there is evidence that bulk stimulation of different descending pathways can activate limb motoneurons in an orderly fashion (Somjen et al., 1965).

So how might less excitable neurons become activated? Studies of reticulospinal networks in adult fish have revealed differences in the participation of reticulospinal neurons during movements of different intensities. In goldfish, sensory stimuli responsible for executing powerful escape responses generate a single action potential in large, Mauthner cells, which provide short latency excitation to large PMns via monosynaptic, chemical connections and disynaptic, electrical ones (Fetcho and Faber, 1988). In lampreys, faster swimming movements evoked by electrical stimulation of the midbrain locomotor region (MLR) are associated with the sequential recruitment of middle (MRRN) and then posterior (PRRN) rhombencephalic reticular nuclei (Brocard and Dubuc, 2003). Studies of identified neurons in the MRRN have revealed dual component electrical/glutamatergic synapses to axial

motoneurons innervating both slow and fast musculature (Buchanan et al., 1987; Rovainen, 1974), as described here for the nMLF. In addition, while neurons in the MRRN increase their tonic firing rates in response to stronger MLR stimulation, neurons in the PRRN fire rhythmically when recruited. The findings in adult fish are consistent with ours in larvae, where tonically active reticulospinal neurons can selectively engage more excitable neurons, and, more important, suggest that less excitable neurons are likely engaged by inputs arriving more concurrently. In this sense, the higher Rin motoneurons act more as integrators, while the lower Rin motoneurons act like coincidence detectors (Konig et al., 1996).

These observations raise the possibility that different sensations generate graded responses via reticular nuclei by regulating their relative activity levels and synchrony of firing. Reticular nuclei are activated by a wide variety of sensory modalities, including somatic, olfactory, acoustic, visual and vestibular sensations (Buhl et al., 2012; Derjean et al., 2010; Huang et al., 2013; Kohashi and Oda, 2008; Orger et al., 2008; Zelenin et al., 2007). In our experiments, the simple light ON/OFF stimulus was not sufficient to get less excitable motoneurons to fire, irrespective of whether inputs derived solely from the nMLF or other potential sources of descending drive. However, recent work using more complex visual stimuli has revealed that more powerful motor output in response to faster drifting gratings is associated with increased activity in the nMLF, not the recruitment of new neurons (Severi et al., co-submission). Since ablation of the large identifiable nMLF neurons eliminates this response, this demonstrates a causal role for the nMLF in generating graded output to visual stimuli. Given the high rates at which these neurons fire, more activity would lead to more synchronization within the nMLF, and thus increase the likelihood that weighted inputs from multiple neurons arrive simultaneously. Thus by varying the relative synchronization of activity within the nMLF, it would be possible to selectively activate different subsets of motoneurons based on their excitability.

While our work was focused on the interactions of the nMLF with axial motoneurons, we cannot rule out the possibility that more powerful responses to visual stimuli are also a function of interactions with other populations of reticulospinal cells or spinal interneurons. Severi et al. have also demonstrated that responses to faster drifting gratings are manifold, with increases in the amplitude of tail bends, increases in the frequencies of tail beats and longer periods of active swimming. Our work suggests that larger amplitude tail beats could be purely a function of direct interactions with axial motor pools. Kinematic studies of freely swimming zebrafish have revealed that increases in tail beat amplitude are sufficient to generate faster swimming, independent of tail beat frequency and episode duration (Green et al., 2011). As we demonstrate, changes in whole field illumination result in more robust firing in SMns and a bilaterally symmetric increase in the variability of motor bursts, such that they more consistently occupy at least 50% of the swim cycle. Although these are ‘fictive’ readouts of motor activity, this pattern is consistent with longer, larger amplitude tail bends driving predominantly forward swimming (Orger et al., 2008). As such nMLF activity superimposed on the rhythmic premotor inputs generating the same frequency of swimming could generate faster speeds. The observed effects on tail-beat frequency and the duration of swim episodes, however, implicate interactions with premotor populations. These effects could be via reticulospinal or spinal neurons (Kimura et al., 2013; Wiggin et

al., 2012). Notably, spinal and reticulospinal neurons in larval zebrafish also demonstrate systematic differences in Rin related to recruitment order (Kinkhabwala et al., 2011; McLean et al., 2007; McLean et al., 2008), and so the pattern we describe here for motoneurons may also be relevant for differential activation of premotor populations.

How might our findings be relevant to studies of mammalian limb motoneurons? Our work focused on evolutionarily conserved source of premotor drive for initiating movements, the reticulospinal system (Dubuc et al., 2008). The sensitivity of limb motoneurons to reticulospinal drive is set not only by Rin, but also by voltage-gated conductances which generate non-linear responses to synaptic inputs (Heckman and Enoka, 2012). These conductances have lower activation thresholds in higher Rin motoneurons than lower ones (Lee and Heckman, 1998, 1999), which reinforce the gradient in intrinsic excitability generated by Rin. In both adult and larval zebrafish, there are also differences in the potential contribution of non-linear membrane properties to motoneuron recruitment (Ampatzis et al., 2013; Menelaou and McLean, 2012). In this sense, the pattern of temporal summation related to membrane time constant we describe here would be enhanced by the non-linear properties of both limb and axial motoneurons. Critically, in both cat and mouse limb motoneurons membrane time constants are also positively correlated with Rin (Burke, 1968; Gustafsson and Pinter, 1984; Manuel et al., 2009; Zengel et al., 1985). Given that $\tau = RC$, this observation can only be explained by systematic increases in specific membrane resistivity (i.e., the density of channels per unit membrane), which outweigh decreases in membrane capacitance associated with smaller size. Also, in cats reticulospinal cells can fire tonically up to 250 Hz prior to the onset of locomotion (Perreault et al., 1993). Collectively, these observations suggest that differences in the sensitivity of motoneurons to tonic inputs imparted by their membrane time constants may be a generalizable mechanism for the graded recruitment of spinal motoneurons by reticulospinal drive.

Experimental Procedures

Detailed experimental procedures are provided in the Supplemental Experimental Procedures. For experiments, 4–6 day old wild-type, *mitfa*−/− (nacre; Lister et al., 1999), or *parg*^{mn2Et} (Balciunas et al., 2004) zebrafish larvae (*Danio rerio*) were obtained from an in-house facility (Aquatic Habitats, Beverly, MA). Nacre mutants were used for brain imaging and electrophysiological experiments, due to their lack of pigment and the resulting ease of visualization. All procedures conform to NIH guidelines regarding animal experimentation and were approved by Northwestern University Institutional Animal Care and Use Committee.

Electrophysiological Recordings

Electrophysiology experiments were performed as described previously (Bhatt et al., 2007; Masino and Fetcho, 2005). Briefly, for spinal motoneuron recordings zebrafish larvae were immobilized in α-bungarotoxin dissolved in extracellular solution (0.1% w/v; composition in mmol/L: 134 NaCl, 2.9 KCl, 1.2 $MgCl_2$, 2.1 $CaCl_2$, 10 HEPES, 10 glucose, adjusted to pH 7.8 with NaOH) and then transferred to a Sylgard lined glass-bottom dish containing extracellular solution, where the skin and muscle overlying 1–2 spinal segments was

carefully dissected away. For nMLF recordings, the head was rotated dorsal-side up and secured with pins, and a small patch of skin at the rostral edge of the left tectum was removed to allow an easier entry to the brain for the recording pipette. The preparation was then transferred to the physiological recording apparatus, comprised of an upright microscope (AxioExaminer, Zeiss) equipped with a 40x/1.0 NA water immersion objective, and two motorized micromanipulators (MPC-200/ROE-200; Sutter Instruments).

For whole-cell recordings, standard wall glass capillaries were pulled to make recording pipettes with resistances between 10–16 MΩ, which were then back-filled with patch solution (composition in mmol/L: 125 K-gluconate, 4 $MgCl_2$, 10 EGTA, 10 HEPES, 4 Na_2ATP, adjusted to pH 7.3 with KOH). Alexa Fluor 568 was included in the patch solution (final concentration 50 μmol/L) to visualize cell morphology at the end of experiments using a cooled CCD camera (Rolera-XR, Q-Imaging). Images were captured using Qcapture Suite imaging software (Q-Imaging). For patch recordings of identified nMLF neurons, descending neurons were first retrogradely labeled with 10% w/v fluorescein (3000MW, Invitrogen) in patch solution injected to the spinal cord at around segment 20 the day before experimentation. To test for monosynaptic connections, the solution was substituted with high divalent ion extracellular solution (composition in mmol/L: 119.1 NaCl, 2.9 KCl, 4.8 $MgCl_2$, 8.4 $CaCl_2$, 10 HEPES, 10 glucose, adjusted to pH 7.8 with NaOH) delivered by a gravity-fed perfusion system. For pharmacological experiments, the glutamate receptor antagonists NBQX and D-AP5 were dissolved in extracellular solution and added to the perfusate (10 μmol/L and 100 μmol/L final concentration, respectively).

For peripheral motor nerve recordings, pipettes were fashioned from the same ones used for whole-cell recording, however the tip was cut to make a 20–50 μm opening. To evoke motor activity, a visual stimulus was provided by a blue light emitting diode (LED, RadioShack, peak emission wavelength: 468nm) triggered by an isolated stimulator (model 2100; A-M Systems; 2.5–3.6 V; duration: 2–10 sec). Blue light was chosen because the dichroic mirror on the confocal microscope used for calcium imaging effectively filters this wavelength out.

Electrophysiological recordings were acquired using a Multiclamp 700B amplifier, a Digidata series 1440A digitizer, and pClamp software (Molecular Devices). Standard corrections for bridge balance and electrode capacitance were applied in current-clamp mode. All electrophysiological data were analyzed using DataView (Heitler, 2009) and custom written MATLAB scripts. Only cells with stable resting membrane potential below −50mV and overshooting action potentials were included in the analysis.

In Vivo Calcium Imaging

In vivo calcium imaging was performed as described previously (McLean et al., 2007). Briefly, to label spinal motoneurons 10% w/v calcium green dextran (3,000 MW, Invitrogen) was pressure injected into one or two segments of ventral musculature close to the mid-body of anesthetized larval zebrafish using a microinjector (Model IM300, Narishige). To label nMLF neurons, calcium green was pressure injected into the spinal cord around muscle segment 20. Fish were placed in a 28 °C incubator overnight to ensure the neurons were retrogradely labeled.

Image acquisition was performed in conjunction with peripheral motor nerve recordings, as described above. The head was rotated dorsal-side up to image the nMLF, while axial motoneurons were imaged from the side. Images were acquired using a 488 nm wavelength laser on a confocal microscope (Zeiss LSM 710) with a Zeiss 40x/1.0 NA water immersion objective and Zen imaging software. The scanning frame rate was between 100–250 ms/frame. A high-resolution Z-stack of the somata of recorded neurons was always taken at the end of the experiment to assess the location of motoneurons in the spinal cord, and nMLF neurons in the midbrain. Calcium transients were analyzed using ImageJ (NIH) and a custom MATLAB script (MathWorks). For 3D image registration, high-resolution Z-stacks from multiple fish were aligned using MATLAB (Koyama et al., 2011) interfaced with the neuronal reconstruction software, Imaris (Bitplane).

Single-Cell Electroporation

Single cell electroporation was performed as described previously (Bhatt et al., 2004). Briefly, nMLF neurons were first retrogradely labeled with 10% w/v fluorescein (in both wild-type and *nacre* larvae) or tetramethylrhodamine 3,000 MW dextran (for *parg*^{mn2Et} larvae) in patch solution and allowed to recover overnight. Larval zebrafish were then anesthetized and embedded dorsal side up in 1.4 % w/v low melting agar in a glass bottomed dish. A drop of MS-222 solution was used to cover the agar to keep the fish anesthetized through the labeling process, which was performed on the confocal microscope. A glass pipette identical to ones used for whole-cell recording was filled with 10% w/v Alexa Fluor 647 (10,000 MW, Invitrogen) in patch solution, and was advanced down to the nMLF using a motorized micromanipulator (MPC-200/ROE-200) until it directly contacted the target neuron. A train of current pulses (2–4 V; pulse duration: 1 ms; pulse interval: 2 ms; total length: 0.5 s) was then applied via an isolated stimulator. A high-resolution Z-stack of the nMLF was taken right after electroporation because the cell body and dendrites filled immediately. The fish was then removed from the agar and left to recover in system water for one hour to allow the dye to fill the axon collaterals. To image axon collaterals in the spinal cord, the fish was immobilized with α-bungarotoxin and embedded on their side in agar. Imaris was used to reconstruct axon collaterals, and MATLAB was used to analyze the length of the reconstructed axon collaterals (Kishore and Fetcho, 2013).

Supplementary Material

Refer to Web version on PubMed Central for supplementary material.

Acknowledgments

This work was supported by a grant from the National Institute of Neurological Disorders and Stroke (R01-NS067299), The Esther A. and Joseph Klingenstein Fund, The Searle Scholars Program, and The Alfred P. Sloan Foundation. We also thank Sandeep Kishore for sharing the MATLAB script for analyzing axon collateral distribution; Indira Raman, CJ Heckman, Melina Hale, Marco Gallio, Kristen Severi, Florian Engert and members of the McLean lab for comments on the manuscript and discussions during the course of this project; Eli Cadoff for technical support; and Matt Chiarelli for fish care.

References

Alstermark B, Isa T. Circuits for skilled reaching and grasping. Annu Rev Neurosci. 2012; 35:559–578. [PubMed: 22524789]

Ampatzis K, Song J, Ausborn J, El Manira A. Pattern of innervation and recruitment of different classes of motoneurons in adult zebrafish. J Neurosci. 2013; 33:10875–10886. [PubMed: 23804107]

Balciunas D, Davidson AE, Sivasubbu S, Hermanson SB, Welle Z, Ekker SC. Enhancer trapping in zebrafish using the Sleeping Beauty transposon. BMC Genomics. 2004; 5:62. [PubMed: 15347431]

Bhatt DH, McLean DL, Hale ME, Fetcho JR. Grading movement strength by changes in firing intensity versus recruitment of spinal interneurons. Neuron. 2007; 53:91–102. [PubMed: 17196533]

Bhatt DH, Otto SJ, Depoister B, Fetcho JR. Cyclic AMP-induced repair of zebrafish spinal circuits. Science. 2004; 305:254–258. [PubMed: 15247482]

Binder MD, Heckman CJ, Powers RK. Relative strengths and distributions of different sources of synaptic input to the motoneurone pool: implications for motor unit recruitment. Adv Exp Med Biol. 2002; 508:207–212. [PubMed: 12171113]

Binder MD, Robinson FR, Powers RK. Distribution of effective synaptic currents in cat triceps surae motoneurons. VI. Contralateral pyramidal tract. J Neurophysiol. 1998; 80:241–248. [PubMed: 9658045]

Borla MA, Palecek B, Budick S, O'Malley DM. Prey capture by larval zebrafish: evidence for fine axial motor control. Brain Behav Evol. 2002; 60:207–229. [PubMed: 12457080]

Brocard F, Dubuc R. Differential contribution of reticulospinal cells to the control of locomotion induced by the mesencephalic locomotor region. J Neurophysiol. 2003; 90:1714–1727. [PubMed: 12736238]

Buchanan JT, Brodin L, Dale N, Grillner S. Reticulospinal neurones activate excitatory amino acid receptors. Brain Res. 1987; 408:321–325. [PubMed: 2885068]

Buhl E, Roberts A, Soffe SR. The role of a trigeminal sensory nucleus in the initiation of locomotion. J Physiol. 2012; 590:2453–2469. [PubMed: 22393253]

Burke RE. Group Ia synaptic input to fast and slow twitch motor units of cat triceps surae. J Physiol. 1968; 196:605–630. [PubMed: 5664234]

Burke RE. The role of synaptic organization in the control of motor unit activity during movement. Prog Brain Res. 1979; 50:61–67. [PubMed: 551456]

Burke RE, Rymer WZ, Walsh JV. Relative strength of synaptic input from short-latency pathways to motor units of defined type in cat medial gastrocnemius. J Neurophysiol. 1976; 39:447–458. [PubMed: 181542]

Cope TC, Pinter MJ. The size principle: Still working after all these years. News in Physiological Sciences. 1995; 10:280–286.

Derjean D, Moussaddy A, Atallah E, St-Pierre M, Auclair F, Chang S, Ren X, Zielinski B, Dubuc R. A novel neural substrate for the transformation of olfactory inputs into motor output. PLoS Biol. 2010; 8:e1000567. [PubMed: 21203583]

Drew T, Prentice S, Schepens B. Cortical and brainstem control of locomotion. Prog Brain Res. 2004; 143:251–261. [PubMed: 14653170]

Dubuc R, Brocard F, Antri M, Fenelon K, Gariepy JF, Smetana R, Menard A, Le Ray D, Viana Di Prisco G, Pearlstein E, et al. Initiation of locomotion in lampreys. Brain Res Rev. 2008; 57:172–182. [PubMed: 17916380]

Eaton RC, Nissanov J, Wieland CM. Differential activation of Mauthner and non-Mauthner startle circuits in the zebrafish - implications for functional substitution. J Comp Physiol A. 1984; 155:813–820.

Enoka RM, Stuart DG. Henneman Size Principle - Current Issues. Trends Neurosci. 1984; 7:226–228.

Fernandes AM, Fero K, Arrenberg AB, Bergeron SA, Driever W, Burgess HA. Deep brain photoreceptors control light-seeking behavior in zebrafish larvae. Curr Biol. 2012; 22:2042–2047. [PubMed: 23000151]

Fetcho JR, Faber DS. Identification of motoneurons and interneurons in the spinal network for escapes initiated by the mauthner cell in goldfish. J Neurosci. 1988; 8:4192–4213. [PubMed: 3183720]

Fetcho JR, O'Malley DM. Visualization of active neural circuitry in the spinal cord of intact zebrafish. J Neurophysiol. 1995; 73:399–406. [PubMed: 7714582]

Frankenhaeuser B, Hodgkin AL. The action of calcium on the electrical properties of squid axons. J Physiol. 1957; 137:218–244. [PubMed: 13449874]

Gahtan E, O'Malley DM. Visually guided injection of identified reticulospinal neurons in zebrafish: a survey of spinal arborization patterns. J Comp Neurol. 2003; 459:186–200. [PubMed: 12640669]

Gahtan E, Tanger P, Baier H. Visual prey capture in larval zebrafish is controlled by identified reticulospinal neurons downstream of the tectum. J Neurosci. 2005; 25:9294–9303. [PubMed: 16207889]

Green MH, Ho RK, Hale ME. Movement and function of the pectoral fins of the larval zebrafish (Danio rerio) during slow swimming. J Exp Biol. 2011; 214:3111–3123. [PubMed: 21865524]

Grillner S, Hongo T, Lund S. The vestibulospinal tract. Effects on alpha-motoneurones in the lumbosacral spinal cord in the cat. Exp Brain Res. 1970; 10:94–120. [PubMed: 5411977]

Grillner S, Hongo T, Lund S. Convergent effects on alpha motoneurones from the vestibulospinal tract and a pathway descending in the medial longitudinal fasciculus. Exp Brain Res. 1971; 12:457–479. [PubMed: 5093725]

Gustafsson B, Pinter MJ. Relations among passive electrical properties of lumbar alpha-motoneurones of the cat. J Physiol. 1984; 356:401–431. [PubMed: 6520792]

Heckman CJ, Enoka RM. Motor unit. Compr Physiol. 2012; 2:2629–2682. [PubMed: 23720261]

Heitler WJ. Practical tools for analysing rhythmic neural activity. J Neurosci Methods. 2009; 185:151–164. [PubMed: 19765613]

Huang KH, Ahrens MB, Dunn TW, Engert F. Spinal projection neurons control turning behaviors in zebrafish. Curr Biol. 2013; 23:1566–1573. [PubMed: 23910662]

Hultborn H, Brownstone RB, Toth TI, Gossard JP. Key mechanisms for setting the input-output gain across the motoneuron pool. Prog Brain Res. 2004; 143:77–95. [PubMed: 14653153]

Kimmel CB, Powell SL, Metcalfe WK. Brain neurons which project to the spinal cord in young larvae of the zebrafish. J Comp Neurol. 1982; 205:112–127. [PubMed: 7076887]

Kimura Y, Okamura Y, Higashijima S. alx, a zebrafish homolog of Chx10, marks ipsilateral descending excitatory interneurons that participate in the regulation of spinal locomotor circuits. J Neurosci. 2006; 26:5684–5697. [PubMed: 16723525]

Kimura Y, Satou C, Fujioka S, Shoji W, Umeda K, Ishizuka T, Yawo H, Higashijima SI. Hindbrain V2a neurons in the excitation of spinal locomotor circuits during zebrafish swimming. Curr Biol. 2013; 23:843–849. [PubMed: 23623549]

Kinkhabwala A, Riley M, Koyama M, Monen J, Satou C, Kimura Y, Higashijima S, Fetcho J. A structural and functional ground plan for neurons in the hindbrain of zebrafish. Proc Natl Acad Sci U S A. 2011; 108:1164–1169. [PubMed: 21199947]

Kishore S, Fetcho JR. Homeostatic regulation of dendritic dynamics in a motor map in vivo. Nat Commun. 2013; 4:2086. [PubMed: 23803587]

Kohashi T, Oda Y. Initiation of Mauthner- or non-Mauthner-mediated fast escape evoked by different modes of sensory input. J Neurosci. 2008; 28:10641–10653. [PubMed: 18923040]

Konig P, Engel AK, Singer W. Integrator or coincidence detector? The role of the cortical neuron revisited. Trends Neurosci. 1996; 19:130–137. [PubMed: 8658595]

Koyama M, Kinkhabwala A, Satou C, Higashijima S, Fetcho J. Mapping a sensory-motor network onto a structural and functional ground plan in the hindbrain. Proc Natl Acad Sci U S A. 2011; 108:1170–1175. [PubMed: 21199937]

Le Ray D, Juvin L, Ryczko D, Dubuc R. Supraspinal control of locomotion: the mesencephalic locomotor region. Prog Brain Res. 2011; 188:51–70. [PubMed: 21333802]

Lee RH, Heckman CJ. Bistability in spinal motoneurons in vivo: systematic variations in persistent inward currents. J Neurophysiol. 1998; 80:583–593. [PubMed: 9705452]

Lee RH, Heckman CJ. Paradoxical effect of QX-314 on persistent inward currents and bistable behavior in spinal motoneurons in vivo. J Neurophysiol. 1999; 82:2518–2527. [PubMed: 10561423]

Lemon RN. Descending pathways in motor control. Annu Rev Neurosci. 2008; 31:195–218. [PubMed: 18558853]

Liao JC, Fetcho JR. Shared versus specialized glycinergic spinal interneurons in axial motor circuits of larval zebrafish. J Neurosci. 2008; 28:12982–12992. [PubMed: 19036991]

Lister JA, Robertson CP, Lepage T, Johnson SL, Raible DW. nacre encodes a zebrafish microphthalmia-related protein that regulates neural-crest-derived pigment cell fate. Development. 1999; 126:3757–3767. [PubMed: 10433906]

Liu KS, Fetcho JR. Laser ablations reveal functional relationships of segmental hindbrain neurons in zebrafish. Neuron. 1999; 23:325–335. [PubMed: 10399938]

Manuel M, Iglesias C, Donnet M, Leroy F, Heckman CJ, Zytnicki D. Fast kinetics, high-frequency oscillations, and subprimary firing range in adult mouse spinal motoneurons. J Neurosci. 2009; 29:11246–11256. [PubMed: 19741131]

Masino MA, Fetcho JR. Fictive swimming motor patterns in wild type and mutant larval zebrafish. J Neurophysiol. 2005; 93:3177–3188. [PubMed: 15673549]

McLean DL, Fan J, Higashijima S, Hale ME, Fetcho JR. A topographic map of recruitment in spinal cord. Nature. 2007; 446:71–75. [PubMed: 17330042]

McLean DL, Masino MA, Koh IY, Lindquist WB, Fetcho JR. Continuous shifts in the active set of spinal interneurons during changes in locomotor speed. Nat Neurosci. 2008; 11:1419–1429. [PubMed: 18997790]

Mendell LM. The size principle: a rule describing the recruitment of motoneurons. J Neurophysiol. 2005; 93:3024–3026. [PubMed: 15914463]

Menelaou E, McLean DL. A gradient in endogenous rhythmicity and oscillatory drive matches recruitment order in an axial motor pool. J Neurosci. 2012; 32:10925–10939. [PubMed: 22875927]

Menelaou E, VanDunk C, McLean DL. Differences in the morphology of spinal V2a neurons reflect their recruitment order during swimming in larval zebrafish. J Comp Neurol. 2014; 522:1232–1248. [PubMed: 24114934]

Myers PZ. Spinal motoneurons of the larval zebrafish. J Comp Neurol. 1985; 236:555–561. [PubMed: 4056102]

Orger MB, Kampff AR, Severi KE, Bollmann JH, Engert F. Control of visually guided behavior by distinct populations of spinal projection neurons. Nat Neurosci. 2008; 11:327–333. [PubMed: 18264094]

Perreault MC, Drew T, Rossignol S. Activity of medullary reticulospinal neurons during fictive locomotion. J Neurophysiol. 1993; 69:2232–2247. [PubMed: 8350141]

Powers RK, Robinson FR, Konodi MA, Binder MD. Distribution of rubrospinal synaptic input to cat triceps surae motoneurons. J Neurophysiol. 1993; 70:1460–1468. [PubMed: 8283207]

Rovainen CM. Synaptic interactions of reticulospinal neurons and nerve cells in the spinal cord of the sea lamprey. J Comp Neurol. 1974; 154:207–223. [PubMed: 4363564]

Sankrithi NS, O'Malley DM. Activation of a multisensory, multifunctional nucleus in the zebrafish midbrain during diverse locomotor behaviors. Neuroscience. 2010; 166:970–993. [PubMed: 20074619]

Severi KE, Portugues RJM, O'Malley DM, Orger MB, Engert F. (co-submission). Behavioral characterization and supraspinal contributions to the neural control of swimming speed in the larval zebrafish.

Somjen G, Carpenter DO, Henneman E. Responses of motoneurons of different sizes to graded stimulation of supraspinal centers of the brain. J Neurophysiol. 1965; 28:958–965. [PubMed: 5867887]

Westcott SL, Powers RK, Robinson FR, Binder MD. Distribution of vestibulospinal synaptic input to cat triceps surae motoneurons. Exp Brain Res. 1995; 107:1–8. [PubMed: 8751056]

Wiggin TD, Anderson TM, Eian J, Peck JH, Masino MA. Episodic swimming in the larval zebrafish is generated by a spatially distributed spinal network with modular functional organization. J Neurophysiol. 2012; 108:925–934. [PubMed: 22572943]

Zelenin PV, Orlovsky GN, Deliagina TG. Sensory-motor transformation by individual command neurons. J Neurosci. 2007; 27:1024–1032. [PubMed: 17267556]

Zengel JE, Reid SA, Sypert GW, Munson JB. Membrane electrical properties and prediction of motor-unit type of medial gastrocnemius motoneurons in the cat. J Neurophysiol. 1985; 53:1323–1344. [PubMed: 3839011]

Highlights

- Midbrain nMLF neurons make direct excitatory connections to spinal motoneurons (Mns)
- Mns exhibit systematic differences in membrane time constants (tau)
- Tonic nMLF input exploits tau to selectively recruit Mns by temporal summation
- nMLF, Mn and behavioral responses to light stimuli support the phenomenon's utility

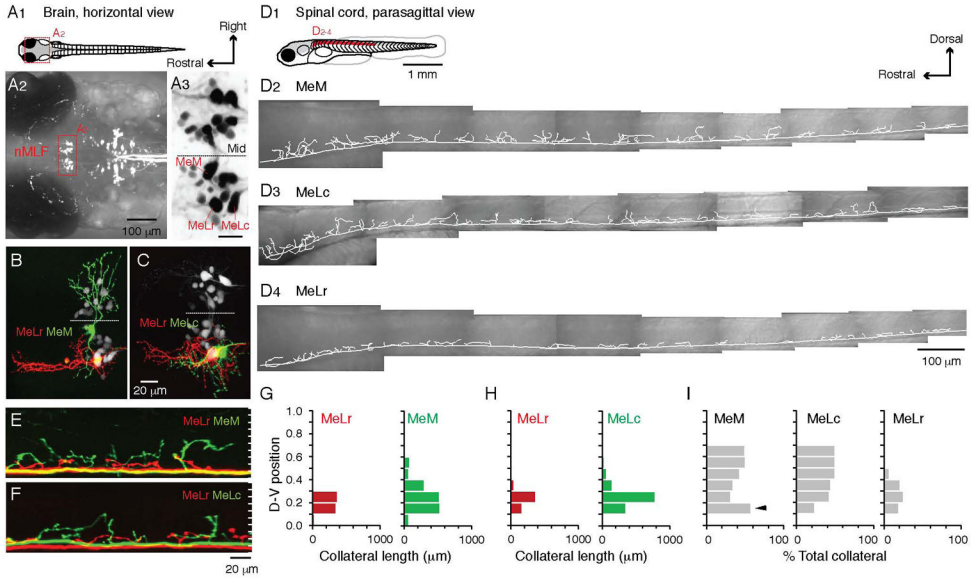

Figure 1. Differences in the Dorso-ventral Distribution of Spinal Axon Collaterals among the Identified nMLF Neurons

(A) A schematic of a larval zebrafish viewed from above (*A1*). The brain area is expanded in *A2* to show the retrogradely labeled descending neurons in the midbrain and hindbrain. The red box highlights the nMLF (nucleus of the medial longitudinal fasciculus). In *A3*, the three large, identified nMLF neurons are marked. Mid = midline. Scale bar = 20 μm.

(B, C) Top-down view of the retrogradely labeled nMLF (white), with two identified nMLF neurons labeled with different colored dyes in the same fish (red and green).

(D) A schematic of a larval zebrafish viewed from the side (*D1*). Lateral view of the reconstructed main axon and collaterals of a MeM (*D2*), MeLc (*D3*), and MeLr (*D4*) neuron in the spinal cord from the region indicated in red on the schematic.

(E, F) Lateral view of the spinal cord with the main axon and collaterals of two identified nMLF neurons labeled with different colored dyes in the same fish. Cells are the same as those presented in *B* and *C*. White tick marks divide the dorso-ventral extent of spinal cord into 10 equal divisions.

(G) Total collateral length from body segments 5–14 at each dorso-ventral division for the MeLr and MeM neurons shown in *B* and *E*, normalized to the top (1) and bottom (0) edges of spinal cord.

(H) As in G, but for the MeLr and MeLc neurons shown in *C* and *F*.

(I) Contribution of MeM, MeLc, and MeLr neurons to the total amount of their spinal collaterals expressed as a percentage. Analysis was restricted to the dorso-ventral divisions 0.2–0.7, where spinal motoneurons are located (n = 5 for each cell type). The MeM neuron contributes more to the total collateral length at division 0.2 (black arrowhead), due to its ventral commissural collaterals.

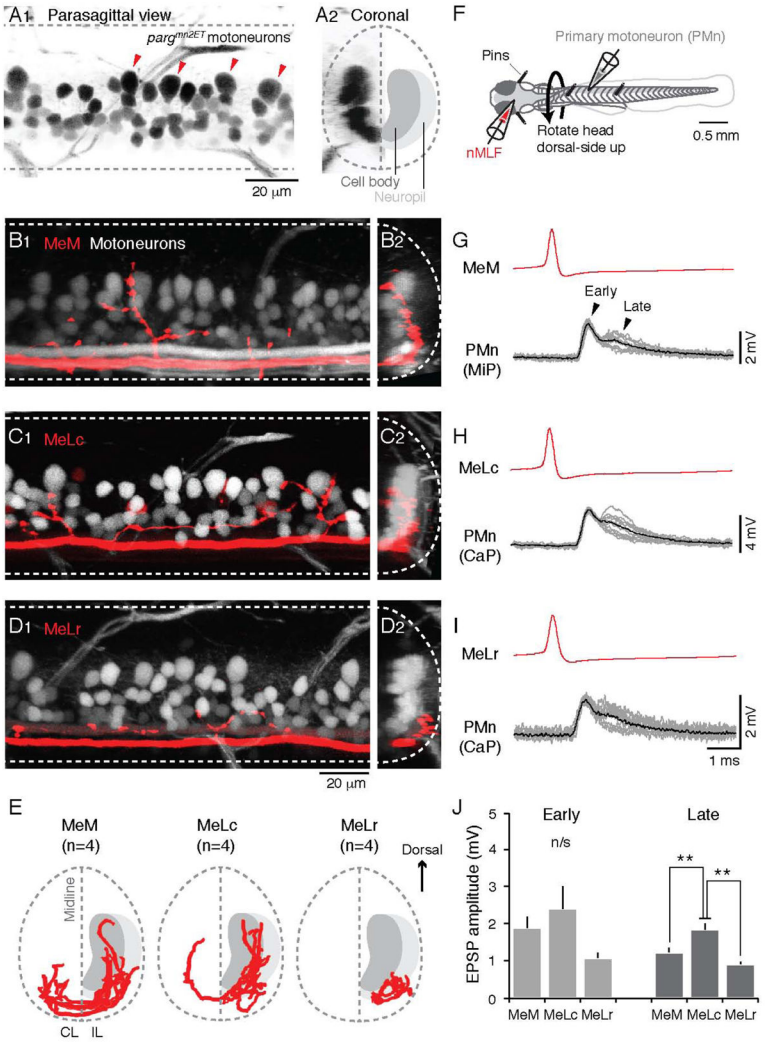

Figure 2. Identified nMLF Neurons Connect to Spinal Motoneurons

(A) Images of the spinal cord of a *parg*^{mn2ET} zebrafish larva, in which GFP is expressed in spinal motoneurons, from the side (*A1*) and in cross-section (*A2*). In *A1*, the four large, dorsally-located primary motoneurons (PMns) in one body segment are marked by red arrowheads. In *A2*, the schematic on the right half demarcates the locations of motoneuron cell bodies and neuropil. Dashed lines indicate the boundary of spinal cord and midline.

(B–D) Confocal Z-stacks of spinal axon collaterals of nMLF neurons (in red) and axial motoneurons (in white) in *parg*^{mn2Et} zebrafish larvae. Images are from the side (*B1–D1*) and in cross section (*B2–D2*). The depth of the Z-stacks is ~20 μm in *B1–D1*. The cross-sectional images in *B2–D2* represent a collapsed view from one body segment (~80–90 μm).

(E) Coronal view of reconstructed axon collaterals from MeM, MeLc, and MeLr neurons registered to anatomical landmarks (n = 4 for each cell type), with the cell body and neuropil layers marked as in *A2*. IL, ipsilateral; CL, contralateral.

(F) Schematic showing the preparation for paired-whole cell patch clamp recordings from nMLF neurons and spinal motoneurons.

(G–I) Example traces from paired recordings from the MeM (*G*), MeLc (*H*) and MeLr (*I*) and a PMn. Individual evoked EPSPs from each pair (gray lines, n = 10 per pair) and an averaged waveform (black line) are temporally aligned to the peak of nMLF action potentials (red, averaged waveform).

(J) Peak amplitude of the early and later components of evoked EPSPs in the PMns. Double asterisks indicate significance (Mann-Whitney U-test with Bonferroni corrections for multiple comparisons, $p<0.05$). n/s = not significant. Here and elsewhere, data are reported as mean +/− SEM.

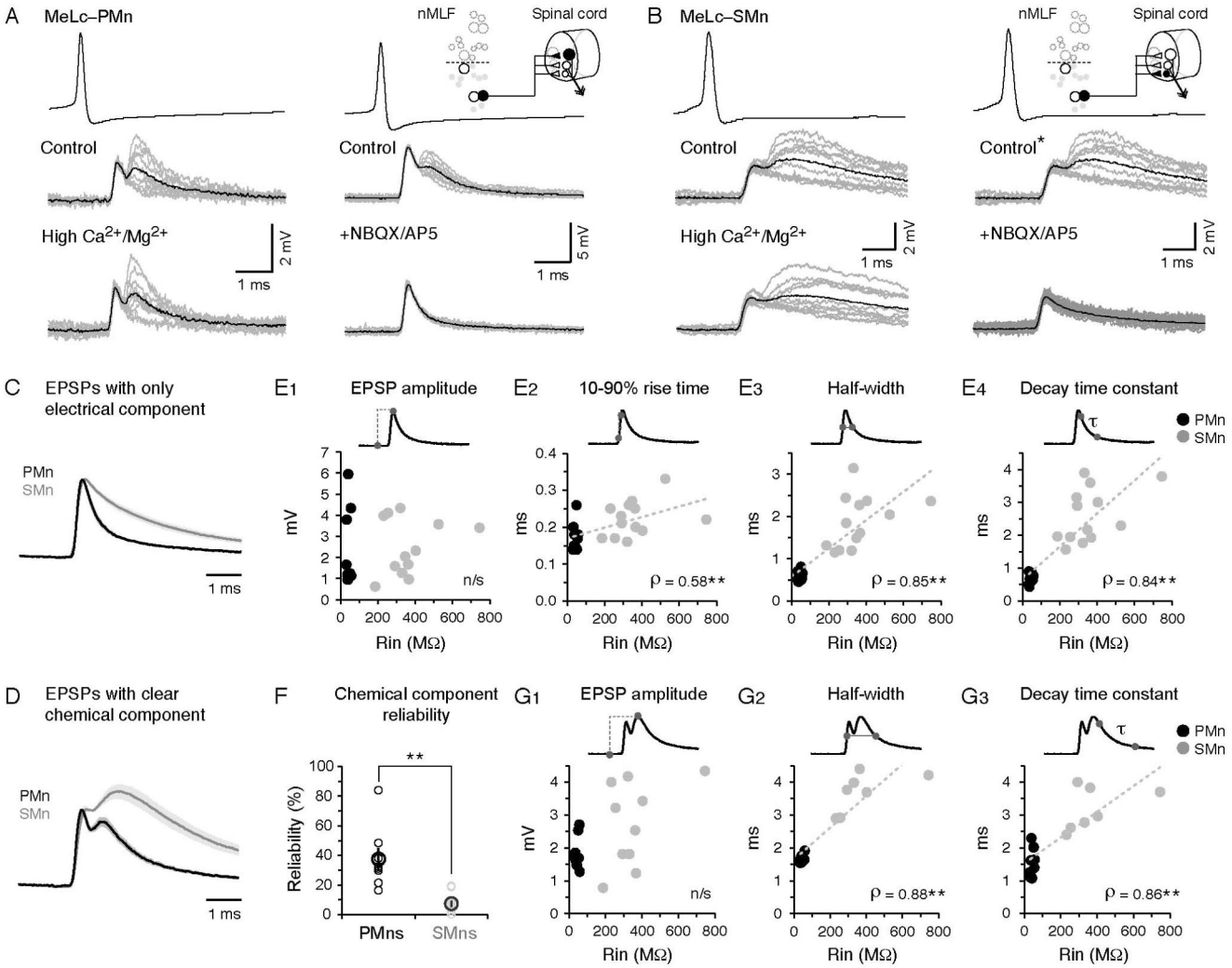

Figure 3. Differences in the Waveforms of MeLc-Evoked EPSPs Related to Motoneuron Input Resistance

(A) Example of direct connections between the MeLc neuron and a larger, dorsal PMn (see schematic in upper right corner) in control solution, high-divalent cation solution (Ca^{2+}/Mg^{2+}), or in the presence of the glutamate receptor antagonists NBQX/AP5. Superimposed EPSPs (gray lines, n = 10) and their averaged trace (black line) are shown in each example.

(B) As in *A*, but direct connections between a MeLc neuron and a smaller, ventral SMn. Note, in this example the control panels and spikes are the same because the hi-divalent and NBQX/AP5 perfusions were performed in the same fish (*).

(C) Comparison of MeLc-evoked EPSPs that contain only the early, electrical component in PMns and SMns. Standard error is indicated by the shading. EPSP waveforms have been scaled and aligned to peaks to illustrate the slower decay in the SMns compared to the PMns.

(D) As in *C*, but for EPSPs that contain a clear chemical component in PMns and SMns.

(E) Properties of MeLc-elicited EPSPs that contain only the early component versus input resistance (Rin) of spinal motoneurons. These include EPSP amplitude (*E1*), rise time (*E2*),

half-width (*E3*), and decay time constant (*E4*). Trend line is a linear fit. **: $p<0.05$ following Spearman's rank test (ρ).

(F) Reliability of the later, chemical component of MeLc-elicited EPSPs in PMns and SMns (PMn, 38 ± 7%, n = 8; SMn, 7 ± 2%, n = 11; Student's t-test, **p<0.05)

(G) As in *E*, but for EPSP amplitude (*G1*), half-width (*G2*) and decay time constant (*G3*) with clear chemical components.

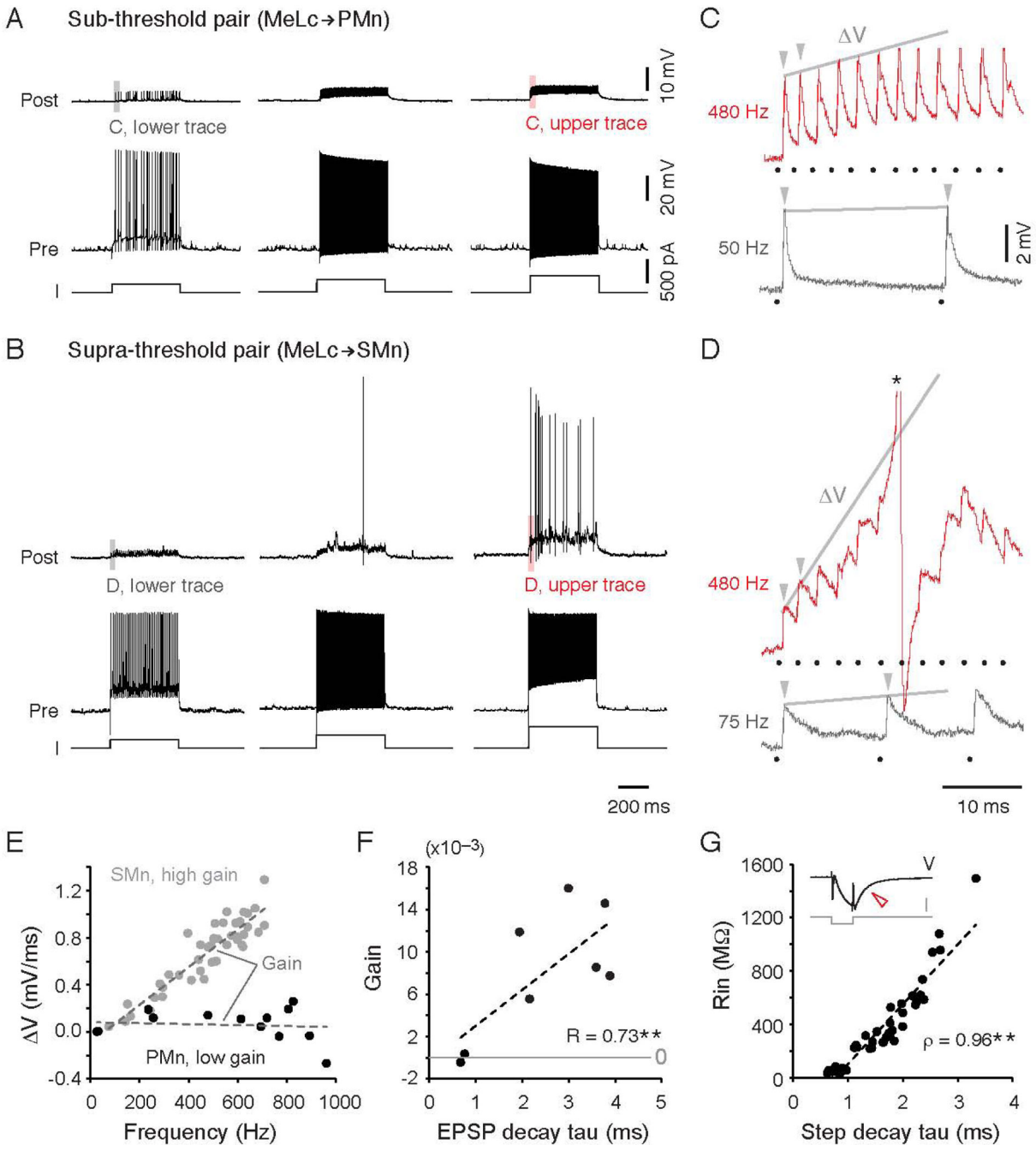

Figure 4. Temporal Summation Enables Higher Rin Motoneurons to Fire

(A) Steps of increasing current levels (I) from left to right lead to increases in instantaneous spike frequency in the MeLc (left, 50 Hz; middle, 255 Hz; right, 480 Hz). MeLc action potentials elicit reliable EPSPs in the connected PMn (Rin = 56 MΩ), which never fires action potentials.

(B) As in *A*, but for a more excitable SMn (Rin = 404 MΩ). Increases in the instantaneous spike frequency of the MeLc (left, 75 Hz; middle, 260 Hz; right, 480 Hz) are sufficient to get the SMn to fire action potentials.

(C) Expanded view of EPSPs evoked by the first two spikes in the current step from the gray (low MeLc firing frequency) and red (high frequency) shaded areas in *A.* The gray line connects the peaks of the first two EPSPs (arrowheads) and the resulting slope (ΔV) was used to calculate EPSP summation at different MeLc firing frequencies. Here, and elsewhere black dots mark the timing of corresponding MeLc action potentials. *C* and *D* share the same scale bars.

(D) As in *C*, but for the SMn illustrated in *B.* Note the much larger ΔV in the top red trace compared to the PMn in *C* at the same MeLc firing frequency. The action potential is truncated (*).

(E) The slope (ΔV) of the first two MeLc elicited EPSPs versus the firing frequency of the corresponding MeLc action potentials for the PMn and SMn shown in *A–D*. The slope of the linearly fit trend lines was used as the gain for EPSP summation for each motoneuron (PMn, R = 0.1; SMn, R = 0.92).

(F) Gain of EPSP summation (the slope of the ΔV trend line as shown in *E*) versus EPSP decay time constant. **: $p<0.05$ following Pearson linear correlation test (R).

(G) Rin versus membrane time constant of spinal motoneurons. The repolarization of the membrane potential (V) after a brief hyperpolarizing current (I) pulse (open red arrowhead) was fit with a single exponential equation to calculate the membrane time constant. Trend line is a linear fit. **: $p<0.05$ following Spearman's rank test (ρ).

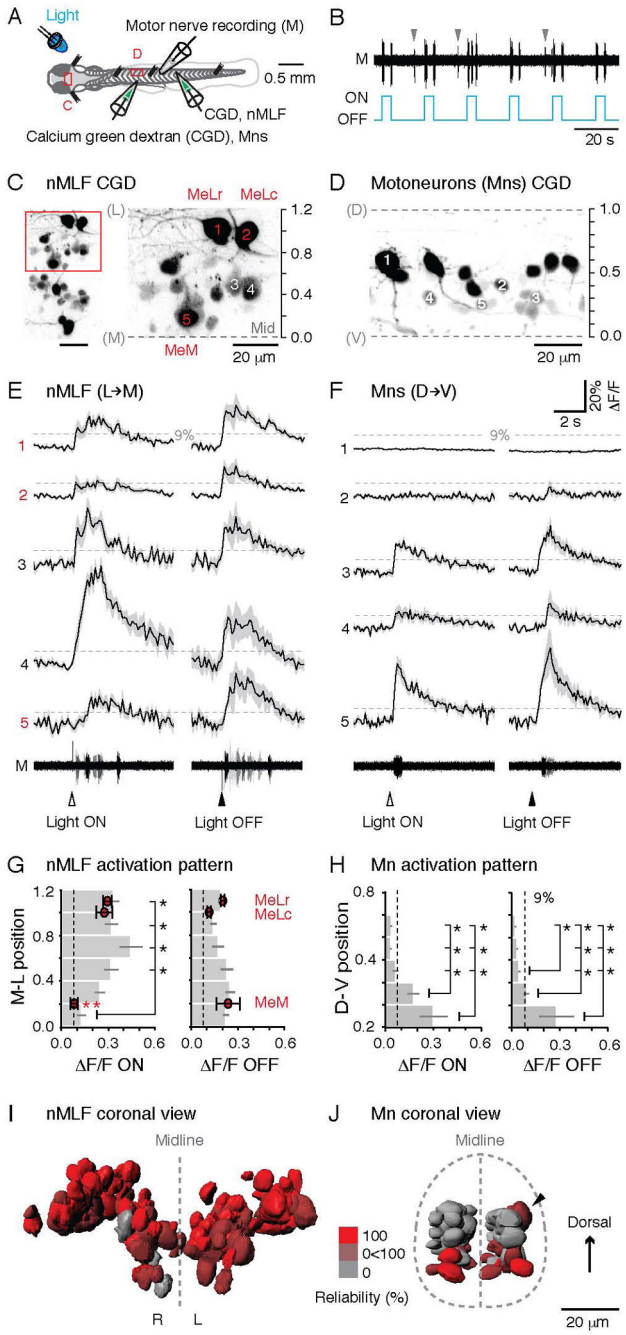

Figure 5. nMLF Neurons Reliably Respond to Changes in Illumination

(A) Schematic showing the preparation for calcium imaging of the nMLF neurons (*C*) or spinal motoneurons (*D*) using calcium green dextran (CGD) injections, and a simultaneous motor nerve (M) recording. LED, light emitting diode.

(B) The onset/offset of the LED reliably elicits ‘fictive’ motor output, which can be recorded from the motor nerve in α-bungarotoxin immobilized preparations. Spontaneous motor output is marked by gray arrowheads.

(C) View of the nMLF neurons backfilled with CGD from above (left), with a higher magnification of the area boxed in red (right). The midline (Mid) of the brain and the center of the MeLr soma were used as references for normalizing the medio-lateral (M-L) locations of nMLF neurons (midline = 0, MeLr soma = 1).

(D) A subset of spinal motoneurons backfilled with CGD. Retrograde filling reliably labels motoneurons throughout the full dorso-ventral (D-V) range of the spinal motor column. Dashed lines mark dorsal (D) and ventral (V) boundaries of the spinal cord, normalized as 1 and 0.

(E) Calcium transients associated with motor output for nMLF neurons at different M-L locations (marked in *C*) in response to light onset and offset (black line = averaged response; shaded area = standard error; n = 5 trials for each neuron). The dashed line marks 9% ΔF/F, the threshold for determining whether a neuron is active. For both *E* and *F*, arrowheads indicate time of the light stimuli. Motor nerve activity (M) for each of the five trials is superimposed in different shades of gray. *E* and *F* share the same scale bars.

(F) Example calcium transients for motoneurons at different D-V locations (marked in *D*) in response to light onset and offset. The dashed line marks 9% ΔF/F.

(G) Averaged calcium response amplitudes of nMLF neurons at different M-L locations in the midbrain. Light ON, n = 91 cells; light OFF, n = 52 cells; both from 8 fish. *: $p<0.05$ following Mann-Whitney U test and Bonferroni correction for multiple comparisons. Response amplitude of the three identified nMLF neurons are shown as red circles at their relative M-L locations. Light ON, n = 25 cells; light OFF, n = 18 cells; both from 8 fish. *: $p<0.05$ following Mann-Whitney U-test and Bonferroni correction for multiple comparisons. In *G* and *H*, dashed line marks the 9% ΔF/F.

(H) Calcium response amplitude to light onset and offset of spinal motoneurons at different D-V locations in the spinal cord. Light ON, n = 127 cells from 11 fish; light OFF, n = 78 cells from 7 fish. *: $p<0.05$ following Mann-Whitney U test and Bonferroni correction for multiple comparisons.

(I) 3D-registration of soma surfaces of nMLF neurons from 8 fish. The neuron surfaces are color-coded according to their reliability of response to light (100%, bright red, always responds to light; 0%, gray, never responds to light). Light onset and offset responses are pooled. R, right side; L, left side.

(J) 3D-registration of soma surfaces of spinal motoneurons from 8 fish. The motoneuron surfaces are color-coded according to their reliability of response to light as described in *J*. A black arrowhead marks a more dorsal motoneuron that responded on the upper side of the side-lying fish.

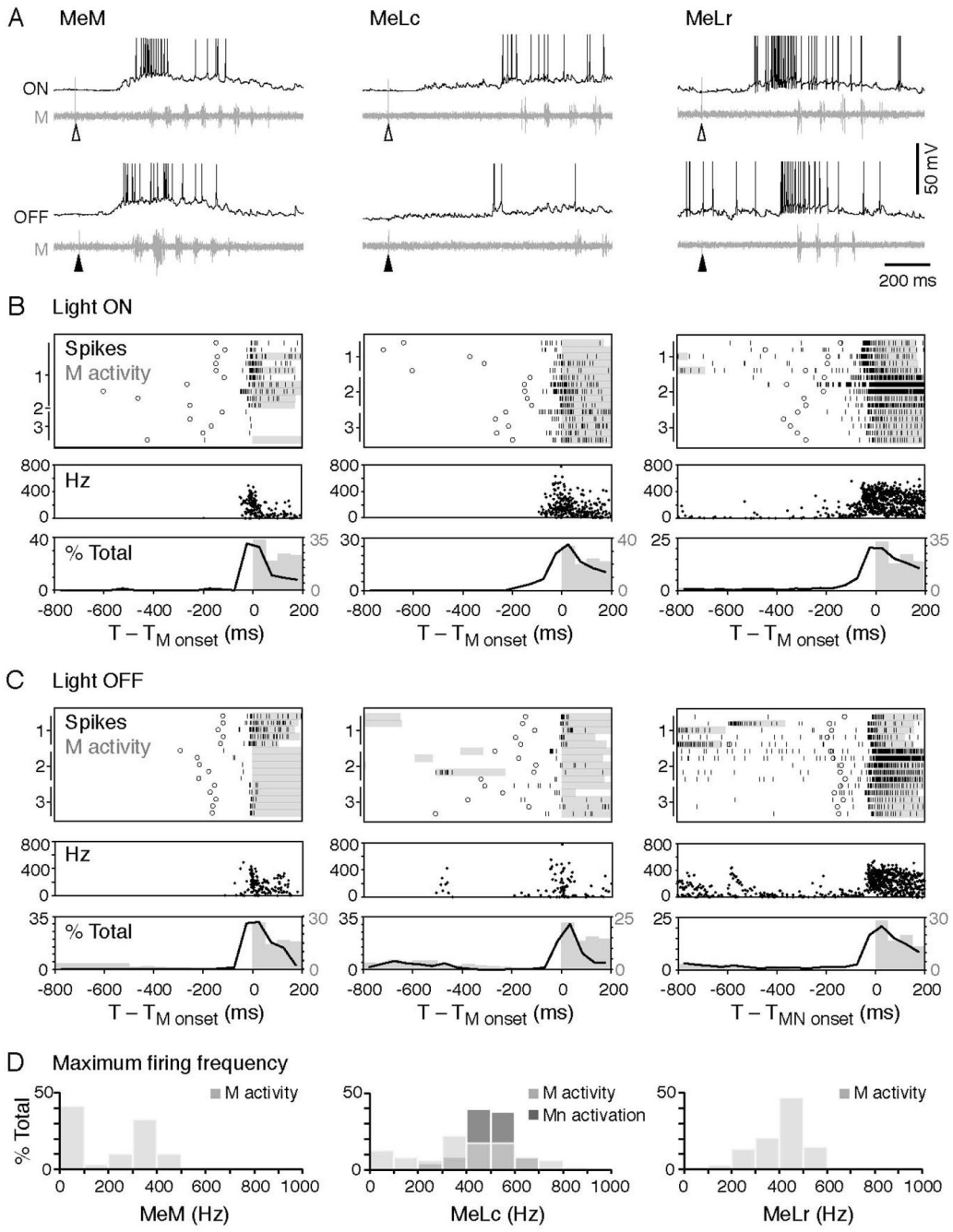

Figure 6. High Frequency Firing of nMLF Neurons Precedes the Motor Response to Changes in Illumination

(A) Example traces of whole-cell recordings on the MeM (left), MeLc (middle), and MeLr (right) neurons together with motor nerve activity in response to light onset (at open arrowheads) and offset (at filled arrowheads). The action potentials of the MeLc and MeLr neurons are truncated.

(B) Upper: raster plots demonstrate the firing pattern of the nMLF neurons in response to light onset (n = 15 trials from 3 neurons in each class, marked on the left of the raster plot). Firing is aligned to the start of the first swim bout (motor nerve activity) after the light

stimulus (black ticks: nMLF action potential, circles: visual stimulus, gray bars: swim bout). Middle: Instantaneous firing frequency of nMLF action potentials shown in the raster plot. Lower: a histogram illustrates the distribution of nMLF action potentials (black line) and motor nerve swim bursts (gray bars). MeM, n = 16 trials from 4 neurons; MeLc, n = 31 trials from 5 neurons; MeLr, n = 34 trials from 5 neurons.

(C) Response to the light offset. Figures are arranged as in *B*. MeM, n = 40 trials from 5 neurons; MeLc, n = 32 trials from 5 neurons; MeLr, n = 33 trials from 5 neurons.

(D) Maximum spike frequency during light evoked swim bouts (M activity; MeM, 58 trials from 5 neurons; MeLc, 63 trials from 5 neurons; MeLr, 68 trials from 7 neurons). The MeLc spike frequencies that successfully activated motoneurons during current injection (Mn activity, illustrated in *4B, D*) fall within the natural spike frequency range of MeLc neurons during swimming. The MeM neuron has more events at the 0–100 Hz frequency bin because in more trials the cell only fires a single action potential in response to light.

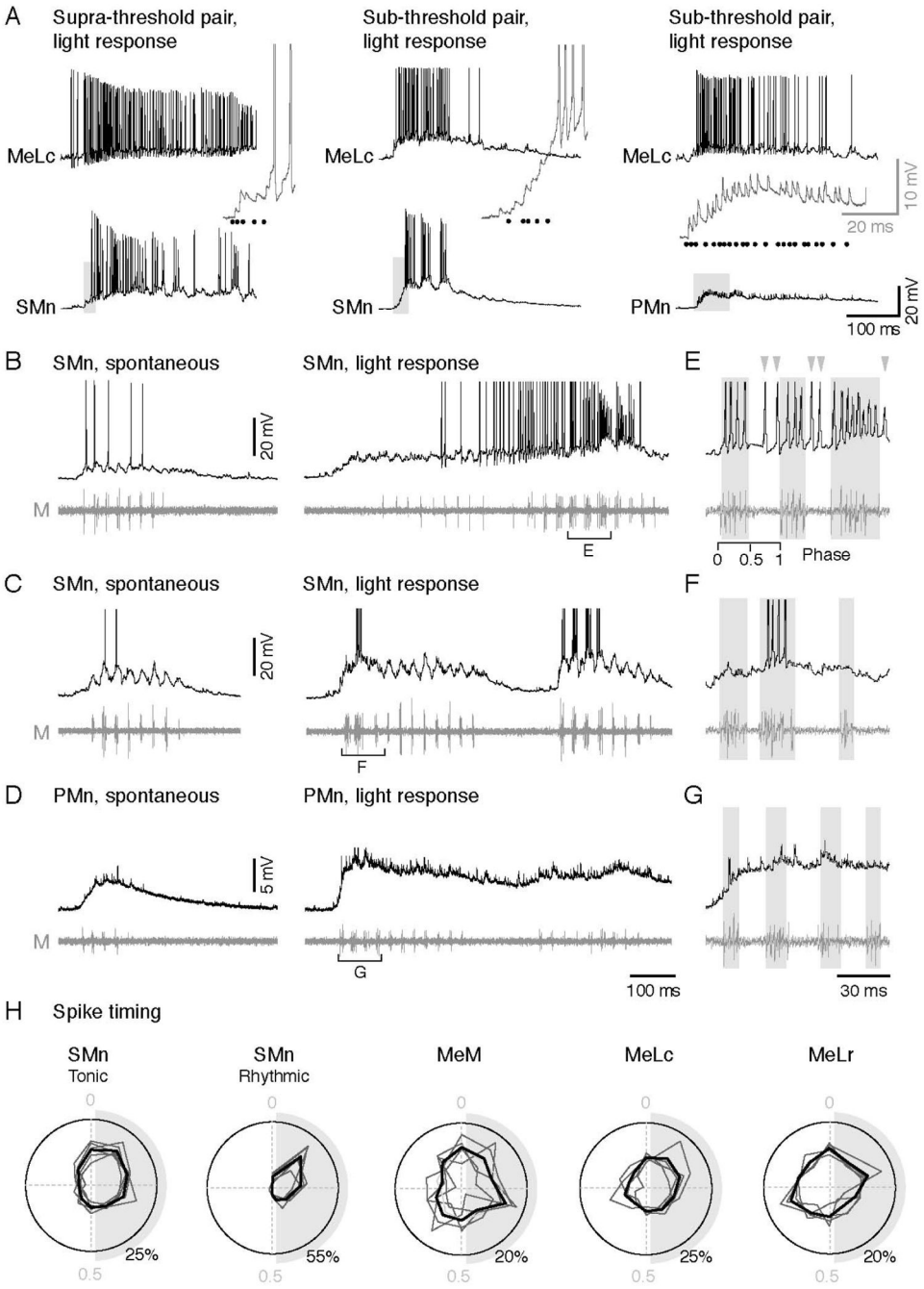

Figure 7. Increased Firing of SMns are Related to Tonic Activity in the nMLF during Light-evoked swimming

(A) Paired-whole cell recordings on the MeLc neuron and spinal motoneurons with different responses to MeLc current injection and light stimulus. Activity shown here is elicited by light. Left: a SMn that can be activated by firing the MeLc alone with current injection (supra-threshold pair). Middle: a SMn that cannot be activated by firing the MeLc alone (sub-threshold pair). Right: a PMn that cannot be activated by firing the MeLc alone. Insets are expanded view from the gray shading areas. MeLc spikes are represented as black dots.

(B–D) Whole-cell recording of SMns (*B*–*C*) and a PMn (*D*) with a motor nerve recording during spontaneous and light evoked swimming.

(E–G) Expanded view from the bracketed areas in *B*–*D* respectively to show phase relationship of action potentials and swimming bursts. Swim bursts are marked by gray shadings to highlight ‘in-phase firing’, while gray arrowheads mark ‘anti-phase’ firing. The phase of a swim cycle (0: start,1: end) is marked in *E*.

(H) Polar plots show the phase relationship of action potentials to cyclical swim bursts during light response normalized to the start (0) and end (1) of the swim cycle (example shown in *E*). Gray shading represents half of the swim cycle. Spike phase distribution of individual cell (dark gray line) and the averaged distribution (black line) are shown. SMns are segregated into groups according to whether their firing pattern was tonic (n= 2,598 spikes from 6 neurons) or rhythmic (n = 435 spikes from 5 neurons). Action potentials of the MeM, MeLc, and MeLr neurons occur throughout the swim cycle consistent with tonic firing behavior (MeM, n = 803 spikes from 5 neurons; MeLc, n = 984 spikes from 4 neurons; MeLr, n = 1071 spikes from 4 neurons).

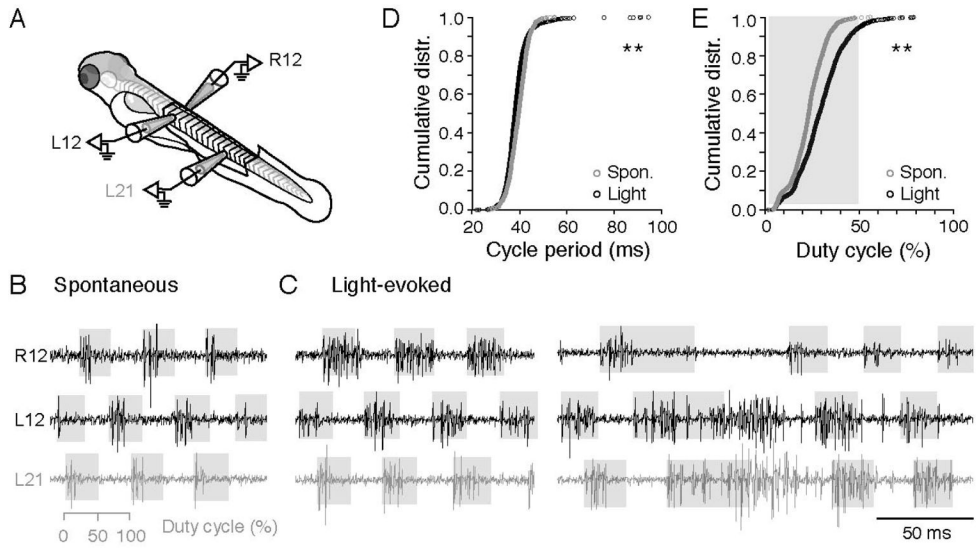

Figure 8. Light-Evoked Behavioral Responses are Primarily Characterized by Increases in the Durations of Alternating Motor Bursts

(A) Schematic of the preparation for recording motor nerves on the left (L) and right (R) sides of the body.

(B) Spontaneous fictive motor bursts recorded at the 12th body segment on the left and right sides, and the 21st body segment on the left side. Shaded gray boxes indicate the 50% duty cycle on a burst-by-burst basis. During spontaneous swimming, motor bursts rarely exceed 50%.

(C) As in *B*, but for light-evoked activity. Fictive swimming in response to light routinely reaches and can exceed a phase value of 0.5.

(D) Cumulative distribution of cycle periods (time between successive motor bursts) for spontaneous and light-evoked motor activity. **: $p<0.05$, Kolmogorov-Smirnov test.

(E) Cumulative distribution of the percentage of the swim cycle motor bursts occupy for spontaneous and light-evoked motor activity. **: $p<0.05$, Kolmogorov-Smirnov test.